Influence of sigma phase precipitation on the impact behaviour of duplex stainless steel pipe fittings

T. Børvik[a,*], L.A. Marken[b], M. Langseth[a], G. Rørvik[b] and O.S. Hopperstad[a]

[a] *Structural Impact Laboratory (SIMLab), Centre for Research-based Innovation (CRI) and Department of Structural Engineering, Norwegian University of Science and Technology, Rich. Birkelands vei 1A, NO-7491 Trondheim, Norway*

[b] *Statoil ASA, Arkitekt Ebbels veg 10, NO-7053 Trondheim, Norway*

Abstract

In this study, the effect of sigma phase precipitation in duplex stainless steel (grade 2205) pipe fittings collected from top-side process systems offshore was investigated under realistic loading conditions. This was done by conducting quasi-static and dynamic impact tests on 3" fittings with nominal outside diameter of 88.9 mm, nominal wall thickness of 3.05 mm and D/t-ratio of nearly 30. The fittings had a sigma phase level between 0 and 15 vol.%, and were loaded by a massive steel indenter with a hemispherical nose of 25 mm radius. In the quasi-static tests, the loading rate was 2 mm/min, while in the dynamic tests the impact velocity was varied between 5 and 10 m/s. A few dynamic impact tests on 2" fittings with an increased wall thickness and low sigma phase levels were carried out for comparison, while some 3" fittings were pre-charged with hydrogen before dynamic testing to examine the effect of sigma phase on cathodic protected subsea components. When the sigma phase level was low (i.e., $\sigma \leq 5$ vol.%), no evidence of fracture was found in any of the pipe fittings, whereas at higher sigma phase levels ($\sigma > 5$ vol.%) fracture occurred in all tests. At the highest sigma phase level ($\sigma \approx 15$ vol.%), extensive fracture and crack growth took place independent of the loading rate.

Keywords: Duplex stainless steel; Sigma phase; Quasi-static tests; Dynamic tests; Fracture

* Corresponding author. Tel.: + 47-73-59-46-47; fax: + 47-73-59-47-01.

E-mail address: tore.borvik@ntnu.no (T. Børvik).

1. Introduction

In a recent study by Børvik et al. (2010), the mechanical properties of pipe fittings in duplex stainless steel (DSS) with deviation in quality caused by sigma phase precipitation were investigated. Such fittings are used both top-side and subsea in large amounts by the offshore industry, and may be exposed to accidental loads such as impacts from dropped objects while in service. Examples of typical DSS pipe fittings are shown in Fig. 1 a), while Fig. 1 b) and c) present micrographs of the material both with and without sigma phase precipitation on the ferrite – austenite boundaries.

The precipitation of sigma was caused by an unintended variation in heat treatment during manufacturing. To achieve the requested mechanical properties the fittings have to be heat treated at 1100 °C after production. However, by mistake the parts were put in a pile instead of being placed on a tray. This caused a variation in temperature between the fittings, and those in the middle of the pile reached temperatures of only about 600 °C. The inadequate heat treatment resulted in sigma phase precipitation during cooling, which may cause a considerable reduction in ductility and impairment in corrosion resistance of the material (see e.g. Nilsson 1992; Kim et al. 1998; Calliari et al. 2006; Cvijovic and Radenkovic 2006; Aursand 2009). Another consequence of this unintended heat treatment was that the level of sigma phase precipitation varied significantly between fittings from the same batch. Approximately 20.000 fittings were produced before the mistake was discovered by chance. Fittings with deviation in quality were detected both in stock and in service by Statoil, and three typical levels of sigma phase precipitation ($\sigma \approx 0$ vol.%, $1 \le \sigma \le 5$ vol.%, $\sigma \approx 10$ vol.%) have been identified based on field inspections offshore.

In Børvik et al. (2010), the effect of sigma phase on the mechanical behaviour of DSS pipe fittings was studied at the material level. This was done by conducting quasi-static and dynamic tensile tests at room ($+20$ °C) and low (-46 °C, -10 °C) temperatures. The fracture toughness

was determined by conducting crack-tip opening displacement (CTOD) tests on single-edge notch bend (SENB) specimens at a temperature of $-10\,°C$, while Charpy impact tests on V-notched specimens were carried out at various temperatures $(-46\,°C,\ -10\,°C,\ +20\,°C)$ to confirm the influence of sigma phase on the impact toughness. It was found that the effect of sigma phase is far less severe with respect to tensile ductility (at low stress triaxiality) than to impact toughness (at high stress triaxiality). It was further observed that the tensile ductility decreased markedly with strain rate, while the influence of temperature was minor. When the material specimens in addition were pre-charged with hydrogen (between 80 and 180 ppm), the tensile ductility was severely reduced independent of sigma phase level. It is therefore of interest to study the effect of sigma phase and hydrogen in real structural components under realistic impact loading conditions.

Several studies have been published in the literature over the years on the behaviour of pipes subjected to accidental loads (see e.g. Jiang et al. 2006; Palmer et al. 2006; Ng and Shen 2006; Jones and Birch 2010; Jones 2010; Manes et al. 2012; Kristoffersen et al. 2013a). These pipes have been empty, filled with a variety of different media or pressurized. Impact against submerged pipelines has been studied by Longva et al. (2013) and Kristoffersen et al. (2013b; 2014). However, none of these studies have investigated the impact properties of pipe fittings with a deviation in quality. It was, therefore, decided to carry out quasi-static and dynamic impact tests on real 3" pipe fittings, having various levels of sigma phase precipitation. A few dynamic impact tests on 2" pipes with increased wall thickness and low sigma phase content were carried out for comparison, while some 3" fittings were pre-charged with hydrogen before dynamic testing to examine the effect of sigma phase on cathodic protected subsea components.

2. Experimental

2.1 Material and test samples

The pipe fittings considered in this study are 3" elbow fittings of class AD200/BD200 or similar, and they are made of duplex stainless steel grade 2205 (UNS S31803; EN 1.4462) with nominal chemical composition 22Cr–5.5Ni–3Mo–0.18N–0.03C (in wt.%). The nominal outside diameter and wall thickness of these fittings are 88.9 mm and 3.05 mm, respectively, according to the API Specification 5L/ISO 3183 standard. This gives a D/t-ratio of nearly 30. The outside diameter was found to remain constant, while the measured wall thickness varied from 3.0 mm to more than 3.5 mm over the circumference. Pipe fittings with four different levels of sigma phase ($\sigma \approx 0$ vol. % , $2 \le \sigma \le 5$ vol.%, $\sigma \approx 8$ vol.% and $\sigma \approx 15$ vol.%) were studied under quasi-static and dynamic loading conditions. In addition, a few dynamic impact tests on 2" fittings with outside diameter of 60.3 mm, wall thickness of 5.5 mm, D/t-ratio of 11 and sigma phase levels between 0 vol.% and 2 vol.% were carried out for comparison, while some 3" fittings were pre-charged with hydrogen. Measured Cauchy stress versus logarithmic strain curves to failure are shown in Fig. 2 for the duplex stainless steel with different levels of sigma phase (Børvik et al. 2010). The influence of the hard and brittle sigma phase into the originally ductile material is a slightly higher tensile stress level and a marked reduction in the strain to failure. Some mechanical data from the quasi-static tensile tests are given in Table 1.

The test samples consisted of three parts: the fitting and two straight pipes, cf. Fig. 3. The three parts were joined together by welding, and the straight pipes and welds were in general without sigma phase precipitation. Pipe systems having fittings with $\sigma \le 5$ vol.% were collected offshore, while heat treatment in an Entech chest-oven was used to reach higher sigma phase levels. The fittings with $\sigma \approx 8$ vol. % were first heat treated and then welded to the pipes, while for the test samples with $\sigma \approx 15$ vol.%, the heat treatment was performed on the whole test sample after welding. Thus, in the latter samples also the straight pipes contained sigma

phase. To study the effect of sigma phase on cathodic protected subsea components, three tests were carried out on hydrogen-charged fittings with a sigma phase level of 0 vol.% and 8 vol.%. Before testing, these fittings were electrically connected to an aluminium anode through a platinum wire attached to the specimen. They were then hydrogen charged in sea water (with a salt content of 3.5 %) at room temperature for more than 6 months. The fittings were tested immediately after pre-charging.

2.2 Test programme and set-up

The test programme is presented in Table 2 and consists of four quasi-static tests (QS1–4) and thirteen dynamic tests (D1–13) at room temperature. As shown in Fig. 3, the fittings were loaded by a massive steel indenter with a hemispherical nose of 25 mm radius and about 120 mm length, while the straight pipes of the test sample were clamped in a steel fixture. The fixture consisted of a thick back plate and two clamps, adjusted to the dimensions of the test sample. The pipes were fixed to the clamps by 6 pre-stressed bolts to obtain clamped end conditions. Owing to the complexity of these experimental tests, only one test was performed for each configuration.

2.3 Quasi-static component tests

The quasi-static component tests were carried out in a 500 kN Dartec servo-hydraulic universal testing machine under displacement control. The maximum actuator stroke of this machine is approximately 100 mm. During testing, the loading rate was set to 2 mm/min, and the force and displacement of the actuator were registered at a logging frequency of 1 Hz. A high-resolution digital camera was used to photograph the local deformation of the pipe fitting at a frequency of 1 picture/mm. To check the clamped support of the pipe, two linear variable

differential transformers (LVDT) were used to measure any axial contraction at the clamps during loading. The details of the set-up for the quasi-static tests are shown in Fig. 4.

2.4 Dynamic tests

Fig. 5a) shows a plan view of the test set-up, while Fig. 5b) provides an overview of the pendulum impactor used in the dynamic tests. The pendulum accelerates a trolley on rails towards the test sample that is fixed to a free-floating reaction wall of 150 tons. The accelerating system consists of an arm that rotates around a set of bearings, i.e., the arm is free to rotate in the plane of Fig. 5b). The arm is open like a crankshaft at the bearing end. The arm itself is connected to a hydraulic/pneumatic actuator system, which provides the moving force. This system accelerates the trolley up to the desired impact velocity. The trolley traverses the length of the rails and subsequently hits the test specimen located at the far end. The maximum working pressure of the accumulator is 200 bar. An initial pressure of 200 bar expanding by 39 litres (from 161 litres to 200 litres) yields an energy output of 720 kJ. However, the trolley leaves the arm after about 2/3 of the stroke, and the maximum energy delivered to the trolley is approximately 500 kJ. More details regarding the operation and the set-up of the pendulum impactor can be found in Hanssen et al. (2003).

The front part of the trolley is equipped with a load cell for measurement of the axial impact force (see Fig. 5a)). The load cell is based on strain gauges that make up the force measuring system. The replaceable nose of the trolley is mounted just in front of the load cell. The impact velocity of the trolley is measured by a photocell system located directly in front of the impact area. In case the test specimen does not have enough capacity to arrest the movement of the trolley itself, a secondary energy absorption system is required. The trolley has solid buffer plates on both sides of the load-cell system. The buffer plates hit crash boxes of extruded aluminium fixed to the reaction wall. This set-up ensures the integrity of the load cell. In these

tests, the trolley impacts the crash boxes after about 100 mm of displacement. The force signal of the load cell is then used to obtain acceleration, velocity, displacement and energy histories of the trolley (Hanssen et al. 2003; Fyllingen et al. 2009).

In addition, the impact process is photographed by two perpendicular and synchronised Photron Fastcam-Ultima APX high-speed video cameras operating at 6000-7500 frames per second with full resolution (1280×800 pixels). It is thus possible to obtain an independent measure of the displacement as a function of time using the images taken with the high-speed camera. Based on the measured force $P(t)$ by the load cell, the acceleration $a(t)$ may be obtained as

$$a(t) = -\frac{P(t)}{m_w} \tag{1}$$

where m_w is the mass of the wagon behind the strain gauges of the load cell. The actual force $F(t)$ acting on the component during testing is found as

$$F(t) = P(t) - m_n a(t) \tag{2}$$

where m_n is the mass of the nose. A combination of Eq. (1) and Eq. (2) gives a relation between the measured and the actual force on the component as

$$F(t) = P(t) - m_n \frac{P(t)}{m_w} = \left(1 - \frac{m_n}{m_w}\right) P(t) = \xi P(t) \tag{3}$$

where ξ is defined as the rigid body load factor. The velocity $v(t)$ and the displacement $u(t)$ are then found by integration of Eq. (1), viz.

$$v(t) = v_i + \int_0^t a(t)\, dt \tag{4}$$

$$u(t) = \int_0^t v(t)\, dt \tag{5}$$

where v_i is the impact velocity. The trolley impacts the buffers at time $t = t_b$. From Eq. (5) the displacement at $t = t_b$ is found from the load cell as $u_{lc}(t_b) = u_{lcb}$. The displacement at $t = t_b$ of

the trolley can also be measured by the high-speed camera as $u_{hsc}(t_b) = u_{hscb}$. Thus, two independent measures of the displacement exist. If it is now assumed that the displacement measured by the high-speed camera is the most accurate, it is possible to adjust the force level measured by the load cell so that the integrated displacement becomes similar to the displacement measured by the high-speed camera system, i.e. $u_{lcb} \approx u_{hscb}$, in an iterative process (see also Hanssen et al. 2003; Hanssen et al. 2005). This approach was adopted here, and even though the resulting corrections were only minor they may be important for later validations of numerical simulations.

The mass of the trolley (including the hemispherical indenter) was 378 kg in all tests. The impact velocity v_i was varied between 5 and 10 m/s, giving a kinetic energy between 4.7 and 18.9 kJ. These levels of kinetic energy are typical for accidental impacts from tools and scaffold parts that may strike and damage offshore process plants from heights up to 15-20 m.

2.5 Verification of sigma phase levels

To verify that the fittings had the expected levels of sigma phase, they were investigated in a light microscope after testing and the amount of sigma phase was determined according to ASTM E662 "Standard Test Method for Determining Volume Fraction by Systematic Manual Point Count". The procedure for the manual point count is described in more detail in Børvik et al. (2010), while both estimated and counted sigma phase levels are given in Table 2. The agreement between the assumed and measured sigma phase levels was judged to be acceptable.

2.6 Measuring of hydrogen content

To measure the hydrogen concentration in the pre-charged pipe fittings (i.e., D11-13), a JUWE H-mat 225 apparatus was used. Immediately after testing, three samples were cut from

the impact zone of the fitting and submerged in liquid nitrogen. The samples were then melted in a graphite crucible in a pulse furnace. During heating and melting, released hydrogen is picked up by a carrier gas flow. A thermal conductivity measuring cell operates as a hydrogen detector, and the hydrogen content is registered. The details in the procedure are described in Børvik et al. (2010), while the results from the measurements are given in Table 2. The total hydrogen content in the sigma-free fittings were found to be about 4 times higher than in the fittings with 8 vol.% sigma, even though the procedure for hydrogen charging was identical. However, the hydrogen content was found to be rather low (3-15 ppm), and somewhat less than the expected hydrogen contents typical for DSS pipe fittings after some years in operation offshore (10-200 ppm – see Johnsen et al. 2009). It is assumed here that the fittings not charged with hydrogen are hydrogen free.

3. Results

3.1 Quasi-static component tests

The force-displacement and energy-displacement curves from the quasi-static tests on 3" fittings with various sigma phase levels are plotted in Fig. 6. These tests are named QS1 to QS4 in Table 2. The energy is calculated as the area under the force-displacement curve. Deformed test samples at the end of the tests (i.e., at a deformation of about 100 mm) are shown in Fig. 7. The hemispherical part of the steel indenter was replaced with a geometrically identical, but stronger, part after the first quasi-static test due to some incipient damage in the nose.

At the lowest sigma phase levels (i.e., $\sigma \approx 0$ vol. % and $2 \le \sigma \le 5$ vol.%), there is no noticeable effect of sigma phase on the force-displacement response and fracture was not found in any of these tests by visual inspection (Fig. 7a)). However, the coating on the pipe fittings peeled off in the most deformed zones. The force-displacement response was unaffected also

for fittings with $\sigma \approx 8$ vol.%, but now a small perpendicular crack was observed at large displacements (Fig. 7b)). The force-displacement curves remained similar even though a significant variation in measured wall thickness of the fittings was found (see Section 2.1).

At $\sigma \approx 15$ vol.%, fracture occurred early and led to the drops in the force-displacement curve seen in Fig. 6. After initial failure the force level increased by about 15 % compared to the tests with less sigma phase. In these tests, also the straight pipes used to fix the test sample to the steel clamps had a sigma phase level equal to that of the fitting (see Section 2.1). The hard and brittle sigma phase gives a higher strain hardening and a reduced ductility in the load-bearing parts of the test sample (see Fig. 2) that corresponds to the increased force and reduced displacement seen in the test. A similar increase in force level was also seen in the dynamic tests on test samples with $\sigma \approx 15$ vol.%, as will be shown in Section 3.2. At this high level of sigma phase, the failure and crack growth were extensive. The test sample was nearly split in two during loading and the fitting partly fragmented (Fig. 7c)).

The LVDT measurements proved that the axial contraction of the pipe ends was negligible in all tests, and it is thus reasonable to consider the pipe as being fully clamped.

3.2 Dynamic component tests

The force-displacement and energy-displacement curves from dynamic tests with impact velocity $v_i = 10$ m/s on 3" fittings with $\sigma \approx 0$ vol.% and $2 \le \sigma \le 5$ vol.% are shown in Fig. 8 (i.e., test D1-D2 in Table 2), while Fig. 9 presents the final deformed shapes of the fittings. The effect of sigma phase on the structural response is small when $2 \le \sigma \le 5$ vol.%. The difference is larger than in the corresponding quasi-static tests, but owing to the lack of duplicate tests it cannot be concluded whether this small difference is significant or not. The force level and energy absorption are also found to be significantly higher in the dynamic tests than in the quasi-static tests (compare Fig. 6 and Fig. 8). Fracture was not seen in these tests by

visual inspection (see Fig. 9), but the coating peeled off. The superimposed oscillations on the measured force-displacement curves in Fig. 8 are due to elastic vibrations of the test component during impact. The same holds for the force-displacement curves presented below. Assuming clamped supports of the specimen, it can be shown by a simple calculation that the fundamental frequency of the system corresponds to a period of approximately 1 ms, which is similar to the measured oscillations. Thus, these oscillations are not due to reflected stress waves in the load cell or multiple impacts.

When the sigma phase level was increased to $\sigma \approx 8$ vol.% (i.e., test D3-D5 in Table 2), fracture occurred in the test sample. Fig. 10 shows a comparison of the force-displacement and energy-displacement curves from these tests, where the impact velocity was varied. It transpires that the force-displacement curves are similar and practically independent of impact velocity until unloading. It should be noted here that the trolley impacted the crash boxes after about 100 mm displacement when the impact velocity was 10 m/s. For lower impact velocities, the trolley rebounded before reaching the crash boxes. Fig. 11 shows the final deformed shape of the fittings after testing at impact velocities between 5 m/s and 10 m/s, while Fig. 12 compares the final shape of the test samples. The fitting was nearly split in two at an impact velocity of 10 m/s, exhibiting quasi-brittle behaviour with fragmentation and extensive crack propagation at low displacements. The crack was arrested at the weld, which was free of sigma phase in these tests. At an impact velocity of 7 m/s, less fracture was seen, but it was still rather severe with a clearly visible hole in the fitting after impact. Only a small crack was seen in the fitting at an impact velocity was 5 m/s, similar to the one observed for quasi-static loading.

As the sigma phase level was further increased to $\sigma \approx 15$ vol.%, i.e., test D6-D7 in Table 2, significant failure occurred at impact and the fitting was nearly split into two parts even at the lowest impact velocity. The behaviour was quasi-brittle with fragmentation and extensive crack propagation which crossed the weld seam. In these tests, the whole test sample was heat

treated to obtain the desired level of sigma phase, which is the reason why the weld was not capable of arresting the running crack. Fig. 13 shows a comparison of the force-displacement and energy-displacement curves from these tests, where the impact velocity was varied. As before, the force-displacement curves are similar and independent of impact velocity until unloading. High-speed camera images of the impact process in test D6 at an impact velocity of 10 m/s are shown in Fig. 14, while the final shapes of the fittings are presented in Fig. 15. These pictures illustrate the extensive amount of fracture in these fittings.

In addition to the tests on 3" pipe fittings, dynamic tests on 2" fittings with increased wall thickness and low sigma phase content were carried out for comparison (test D8-D10 in Table 2). Also in these tests the effect of sigma phase on the structural response was found to be small as long as the sigma content was moderate. The force-displacement curves were independent of both impact velocity and sigma phase level until unloading. Fracture was not observed by visual inspection in any of these tests, and the local damage was small compared to the 3" pipe systems even though the global deformation was large. It is thus believed that these pipes have a significant residual strength after testing even for the highest impact velocities.

Finally, Fig. 16a) gives a comparison of measured force-displacement curves for the hydrogen-charged fittings, i.e., test D11-D13 in Table 2. As already indicated the amount of hydrogen in these fittings was somewhat low, and the effect on the behaviour at low impact velocities was found to be minor (if compared to corresponding curves in Fig. 10). In the hydrogen-charged fitting with 8% sigma, i.e., test D11, a surface crack similar to that observed in test D5 was seen. At an impact velocity of 7 m/s, i.e., test D12, significant fracture occurred in the hydrogen-charged fitting with 8% sigma phase, and the component was quasi-brittle with fragmentation and severe crack propagation (see Fig. 16b)). The crack propagation was arrested at the welds. The fracture appeared more severe than in a similar test on a fitting not charged with hydrogen (Fig. 11b)). In the hydrogen-charged fitting with 0% sigma, i.e., test D13, no fracture was seen at an impact velocity of 5 m/s.

4. Discussion and conclusions

In this study, the effect of sigma phase in duplex stainless steel (grade 2205) pipe fittings collected from top-side process systems offshore has been investigated under realistic loading conditions. This was done by conducting quasi-static and dynamic impact tests on 3" fittings with different levels of sigma phase precipitation. In addition, some dynamic impact tests on 2" fittings and hydrogen-charged 3" fittings were carried out for comparison.

A comparison of force-displacement curves and energy-displacement curves from impact tests on 3" pipe fittings with various sigma phase levels at constant impact velocity of 10 m/s is shown in Fig. 17. Except for the somewhat higher force level at $\sigma \approx 15$ vol.%, the force-displacement curves are similar and independent of sigma phase level. Similar results were obtained for the quasi-static tests as presented in Fig. 6. However, the ductility of the material during impact differs significantly. It was found that when the sigma phase level is low $(2 \le \sigma \le 5$ vol.%), fracture did not take place in any of the tests, while at higher sigma phase levels fracture occurred in all tests. At the highest sigma phase level ($\sigma \approx 15$ vol.%), the fracture was considerable with extensive fracturing and fragmentation independent of the impact velocity.

It is also of interest to compare the energy absorption of the components during impact. At an impact velocity of 10 m/s, it is seen from Fig. 17 that the energy absorption during impact in the component is rather constant and about 16 kJ. However, the test sample with $\sigma \approx 15$ vol.%, where considerable crack propagation and fracture appeared, dissipated less than 14 kJ of energy during the impact. It is important to keep in mind that the impact tests reported here are in practice over after a displacement of about 100 mm, since the trolley then impacts the solid buffers (or the secondary energy absorbers) shown in Fig. 5a). After that, it is no longer possible to distinguish between the energy dissipated by the test samples and the buffers using the set-up applied in this study.

The force-displacement curves from impact tests at 5 m/s on hydrogen-charged fittings with or without sigma are similar. These curves are also similar to the curves from corresponding tests on fittings without hydrogen. The results indicate that neither moderate sigma phase levels nor low hydrogen contents have any important influence on the impact resistance of the DSS fittings. These results are somewhat unexpected, taking the large effect of sigma and hydrogen on the ductility of the DSS at material level into account (Børvik et al. 2010). When increasing the impact velocity to 7 m/s (i.e., doubling the impact kinetic energy), the force level is slightly increased, but now the fitting showed significant fracture upon impact.

As already indicated in Section 3.2, a distinct increase in force level and energy absorption is found in the dynamic tests compared to the quasi-static tests (compare Fig. 6 and Fig. 17). As an example, the test sample with $\sigma \approx 15$ vol.% dissipated only about 8 kJ of energy in the quasi-static tests while 14 kJ of energy was dissipated in the dynamic test, giving an increase in energy absorption of 75%. There may be several reasons for this increase, such as inertia effects, strain rate sensitivity, and a change in deformation and failure mode when going from quasi-static to dynamic loading. In Børvik et al. (2010), an increase in flow stress of about 30% was found for this material when the strain rate was increased from 5×10^{-4} s^{-1} to 50 s^{-1} based on uniaxial tensile tests.

Based on the detailed material investigation on DSS pipe fittings with deviation in quality caused by sigma phase precipitation presented in Børvik et al. (2010), it was concluded that the effect of sigma phase is far less severe with respect to tensile ductility (at low stress triaxiality) than to impact toughness (at high stress triaxiality). It was further found that the tensile ductility decreased markedly with strain rate. When the material specimens in addition were pre-charged with hydrogen, a severe reduction in tensile ductility independent of sigma phase level was observed. These findings at materials level are in general confirmed by the component tests. When the stress triaxiality is low, as in the impact tests presented in this study, pipe fittings

with moderate sigma phase levels can absorb considerable amounts of energy before they fail. The energy imposed in these impact tests is equivalent to a mass of 100 kg dropped from a height of about 20 m, and such impact scenarios are realistic for top-side installations offshore.

References

Aursand M. 2009. Literature review – Intermetallic phases in duplex stainless steel. Technical report MAT-2009053 (Rev.1), StatoilHydro ASA.

Børvik T, Lange H, Marken LA, Langseth M, Hopperstad OS, Aursand M, Rørvik G. 2010. Pipe fittings in duplex stainless steel with deviation in quality caused by sigma phase precipitation. Materials Science and Engineering A 527:6945-6955.

Calliari I, Zanesco M, Ramous E. 2006. Influence of isothermal aging on secondary phases precipitation and toughness of a duplex stainless steel SAF 2205. Journal of Materials Science 41:7643-7649.

Cvijovic Z, Radenkovic G. 2006. Microstructure and pitting corrosion resistance of annealed duplex stainless steel. Corrosion Science 48:3887-3906.

Fyllingen Ø, Hopperstad OS, Langseth M. 2009. Robustness study on the behaviour of top-hat thin-walled high-strength steel sections subjected to axial crushing. International Journal of Impact Engineering 36:12-24.

Hanssen AG, Auestad T, Tryland T, Langseth M. 2003. The kicking machine: A device for impact testing of structural components. International Journal of Crashworthiness 8:385-392.

Hanssen AG, Auestad T, Langseth M, Tryland T. 2005. Development of a 3-component load cell for structural impact testing. International Journal of Mechanics and Materials in Design 2:15-22.

Jiang P, Wang W, Zhang GJ. 2006. Size effects in the axial tearing of circular tubes during quasi-static and impact loadings. International Journal of Impact Engineering 32:2048-2065.

Johnsen R, Nyhus B, Wästberg S. 2009. Hydrogen induced stress cracking (HISC) of stainless steels under cathodic protection in seawater – Presentation of a new test method. Paper no. OMAE2009-79325, OMAE Honolulu, Hawaii USA.

Jones N, Birch RS. 2010. Low-velocity impact of pressurised pipelines. International Journal of Impact Engineering 37:207–219.

Jones N. 2010. Inelastic response of structures due to large impact and blast loadings. The Journal of Strain Analysis for Engineering Design 45:451-464.

Kim SB, Paik KW, Kim YG. 1998. Effect of Mo substitution by W on high temperature embrittlement characteristics in duplex stainless steels. Materials Science and Engineering A 257:67-74.

Kristoffersen M, Børvik T, Westermann I, Langseth M, Hopperstad OS. 2013a. Impact against X65 steel pipes – An experimental investigation. International Journal of Solids and Structures 50:3430-3445.

Kristoffersen M, Casadei F, Børvik T, Langseth M, Solomos G, Hopperstad OS. 2013b. Numerical simulations of submerged and pressurised X65 steel pipes. Proceedings of 12th International Conference on Computational Plasticity, COMPLASXII, Barcelona, Spain, September 3-5.

Kristoffersen M, Casadei F, Børvik T, Langseth M, Hopperstad OS. 2014. Impact against empty and water-filled X65 steel pipes – Experiments and simulations. International Journal of Impact Engineering 71:73-88.

Longva V, Sævik S, Levold E, Ilstad H. 2013. Dynamic simulation of subsea pipeline and trawl board pull-over interaction. Marine Structures 34:156-184.

Manes A, Porcaro R, Ilstad H, Levold E, Langseth M, Børvik T. 2012. The behaviour of an offshore steel pipeline material subjected to bending and stretching. Ships and Offshore Structures 7:371-387.

Ng CS, Shen WQ. 2006. Effect of lateral impact loads on failure of pressurised pipelines supported by foundation. Proceedings of the Institution of Mechanical Engineers 220 (E), pp. 193–206.

Nilsson JO. 1992. Super duplex stainless steels. Materials Science and Technology 8:685-700.

Palmer A, Touhey M, Holder S, Anderson M, Booth S. 2006. Full-scale impact tests on pipelines. International Journal of Impact Engineering 32:1267-1283.

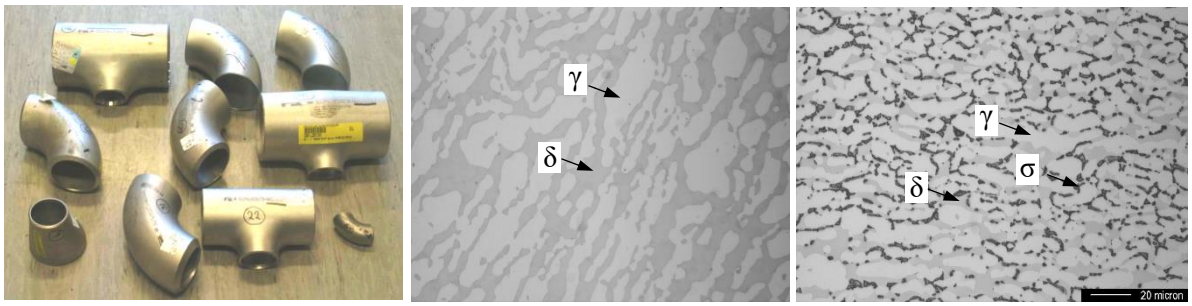

a) b) c)

Fig. 1. a) Typical DSS pipe fittings used by the offshore industry and micrographs of the material with b) 0 vol.% sigma (σ) phase precipitation and c) 14.9 vol.% sigma (σ) phase precipitation on the ferrite (δ) - austenite (γ) boundaries.

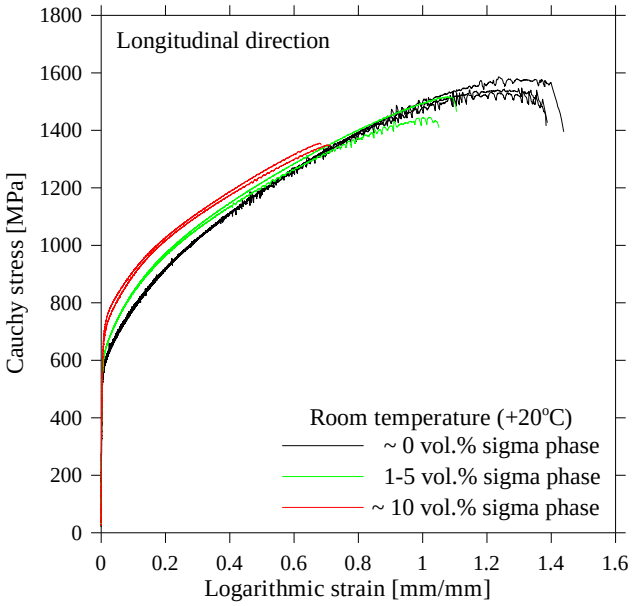

Fig. 2. Cauchy stress versus logarithmic strain curves from quasi-static tensile tests at room temperature for DSS with different levels of sigma phase (Børvik et al. 2010).

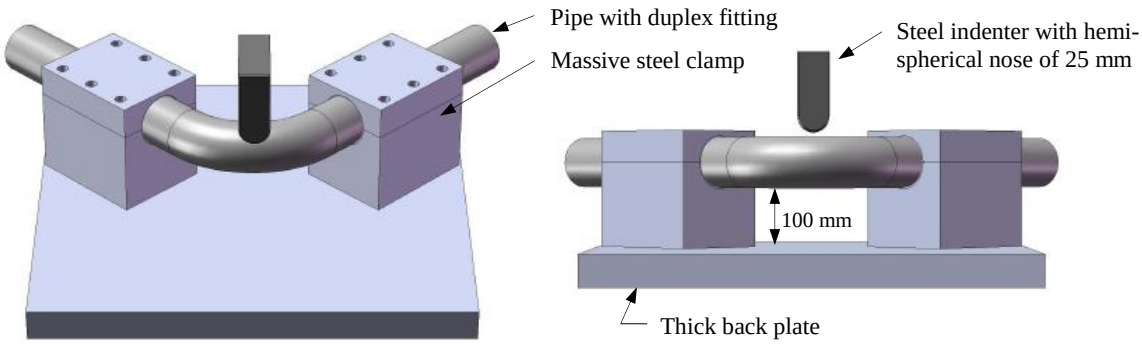

a) Principle of fixture

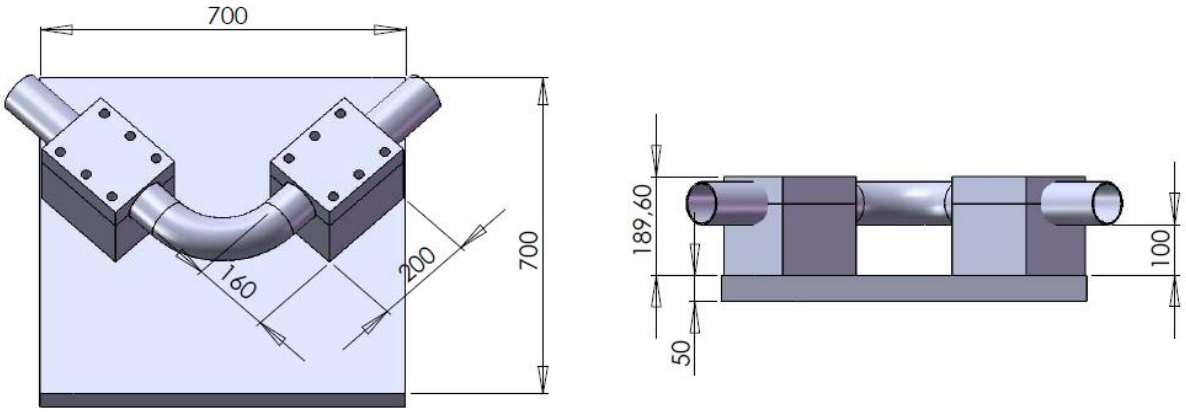

b) Dimensions of fixture

Fig. 3. Fixture used in quasi-static and dynamic tests.

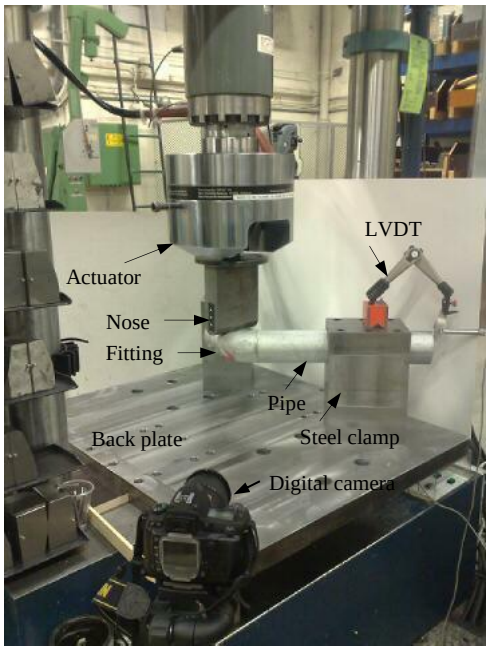

Fig. 4. Test set-up used for the quasi-static tests.

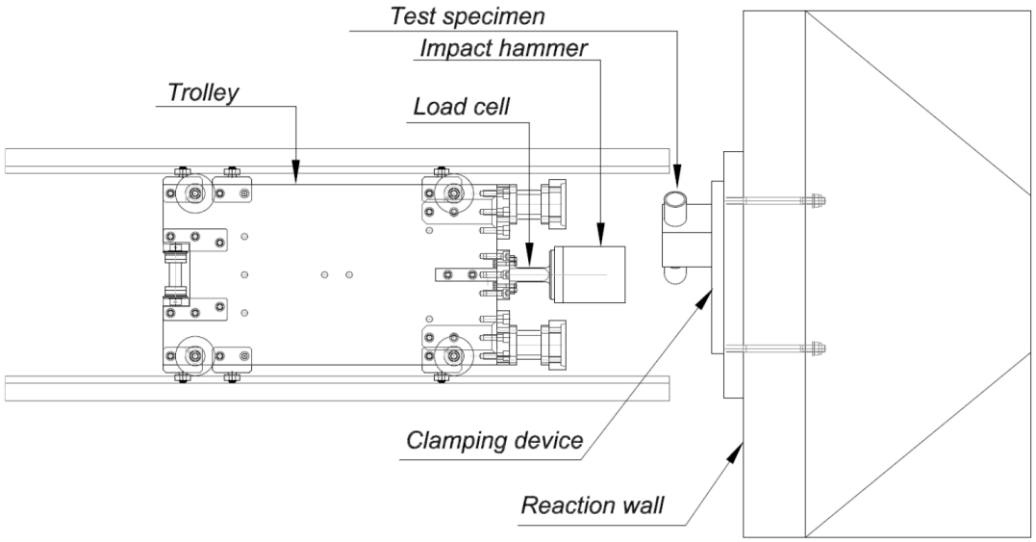

a)

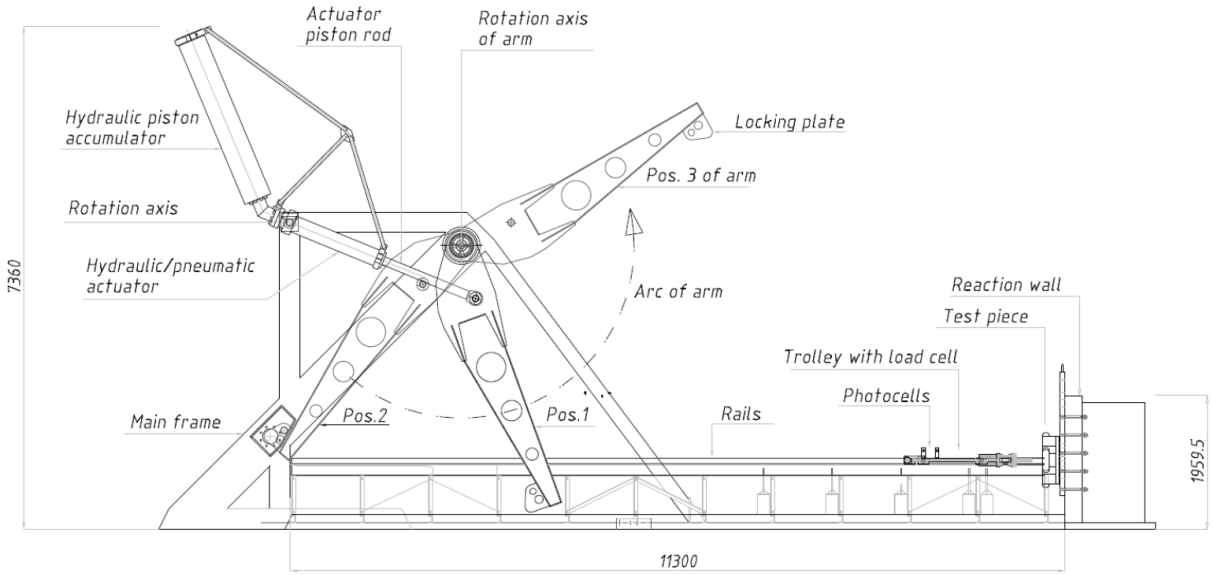

b)

Fig. 5. Test set-up in the pendulum impactor used for the dynamic tests with specimen mounted: a) Plan view and b) side view.

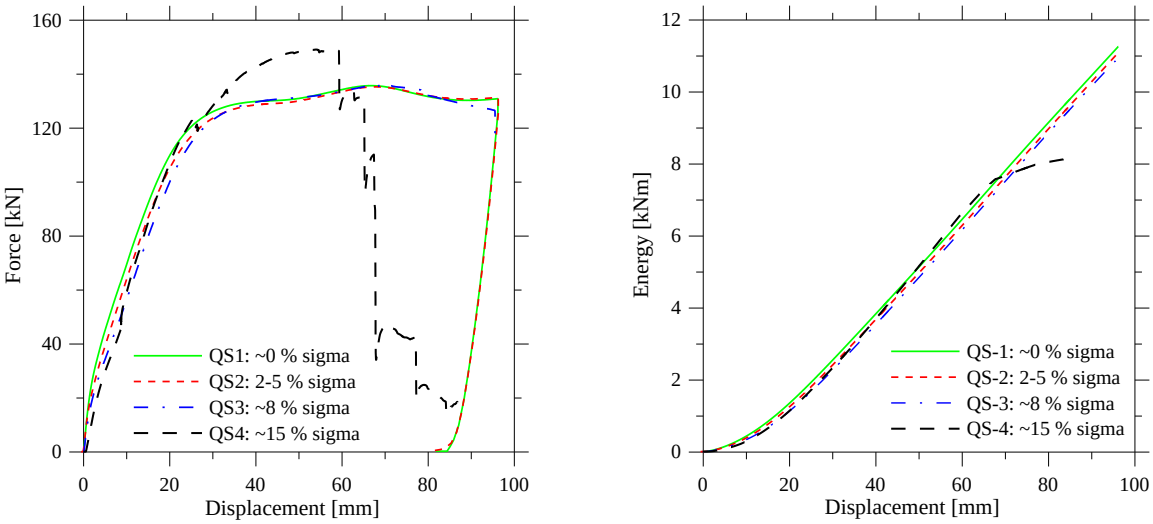

Fig. 6. Force-displacement and energy-displacement curves from quasi-static tests on 3" fittings with various sigma phase levels.

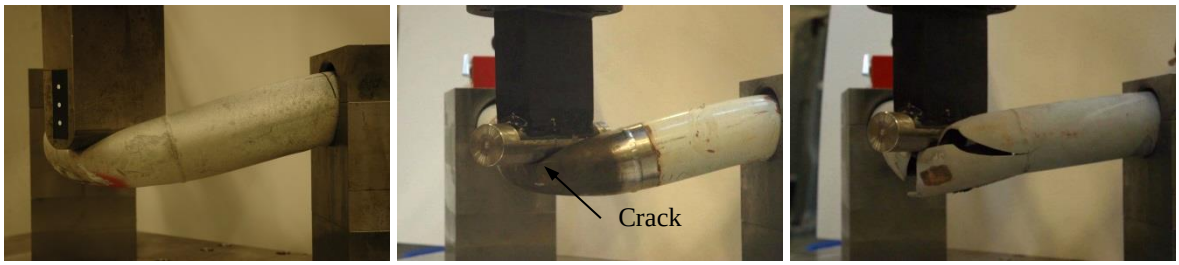

a) b) c)

Fig. 7. Final deformed shape of fittings after quasi-static testing: a) Test QS1 ($\sigma \approx 0$ vol%); b) Test QS3 ($\sigma \approx 8$ vol%); c) Test QS4 ($\sigma \approx 15$ vol%).

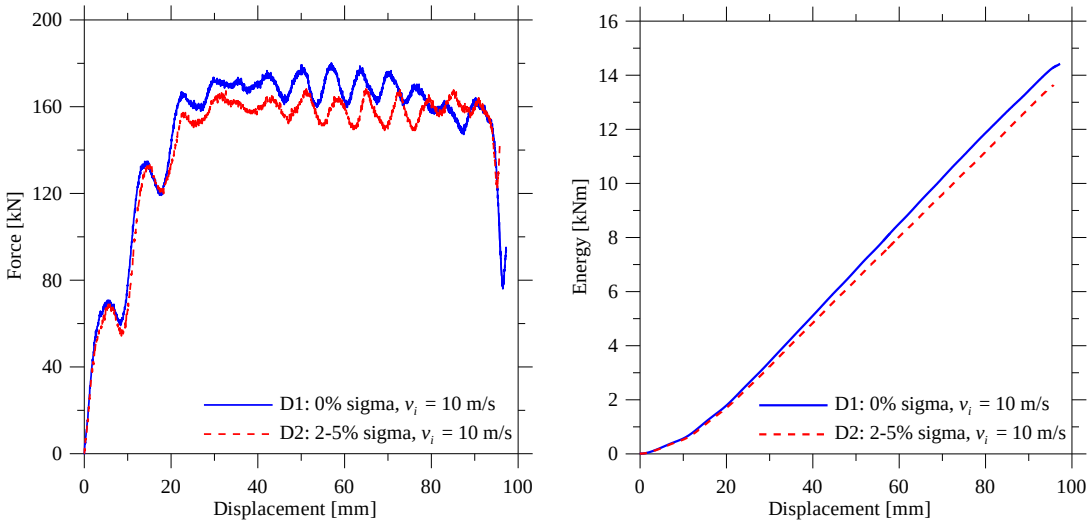

Fig. 8. Force-displacement and energy-displacement curves from test D1 and D2 with impact velocity $v_i = 10$ m/s .

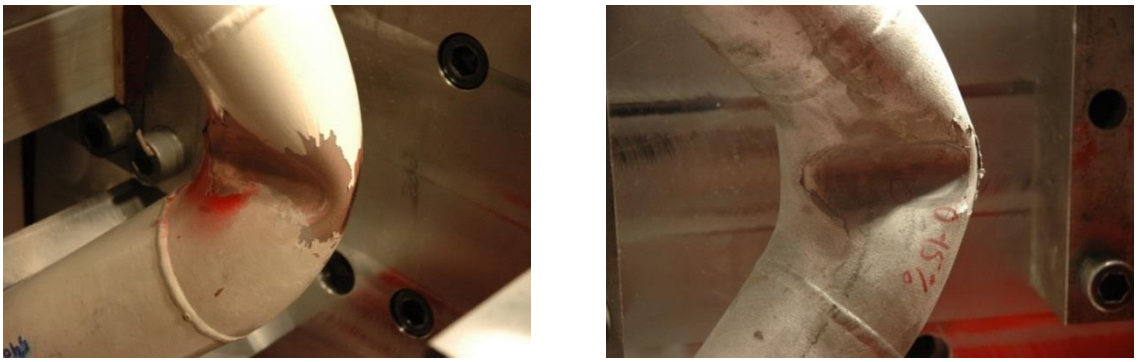

a) b)

Fig. 9. Final deformed shape of fittings after dynamic testing: a) Test D1 ($\sigma \approx 0$ vol%); b) Test D2 ($\sigma \approx$ 2-5 vol%).

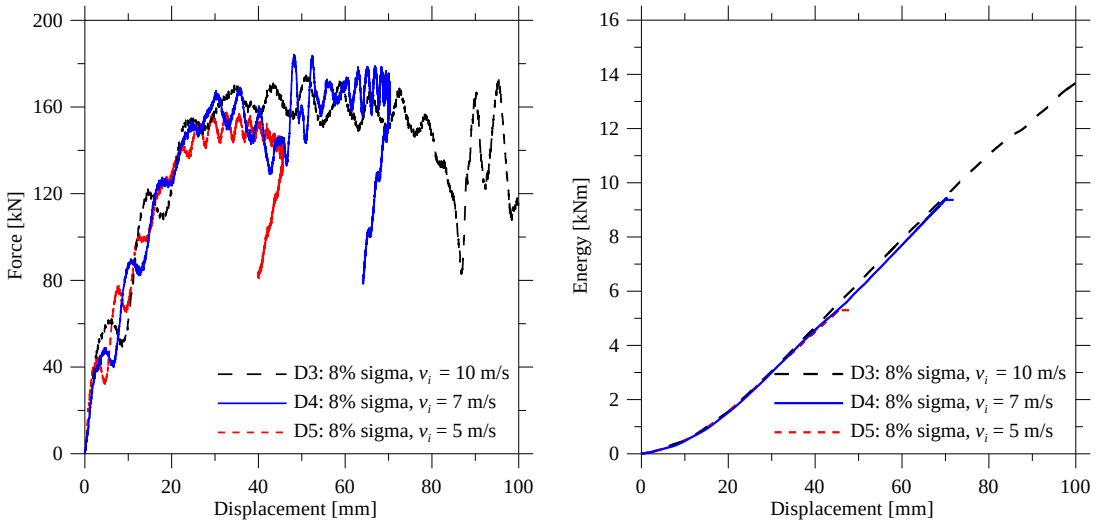

Fig. 10. Force-displacement and energy-displacement curves from test D3, D4 and D5 at impact velocities between 5 m/s and 10 m/s.

a) b) c)

Fig. 11. Final deformed shape of fittings after dynamic testing: a) Test D3 ($\sigma \approx 8$ vol%, $v_i = 10$ m/s); b) Test D4 ($\sigma \approx 8$ vol%, $v_i = 7$ m/s); c) Test D5 ($\sigma \approx 8$ vol%, $v_i = 5$ m/s).

Fig. 12. Test samples with $\sigma \approx 8$ vol% after dynamic testing at various impact velocities (tests D3, D4 and D5).

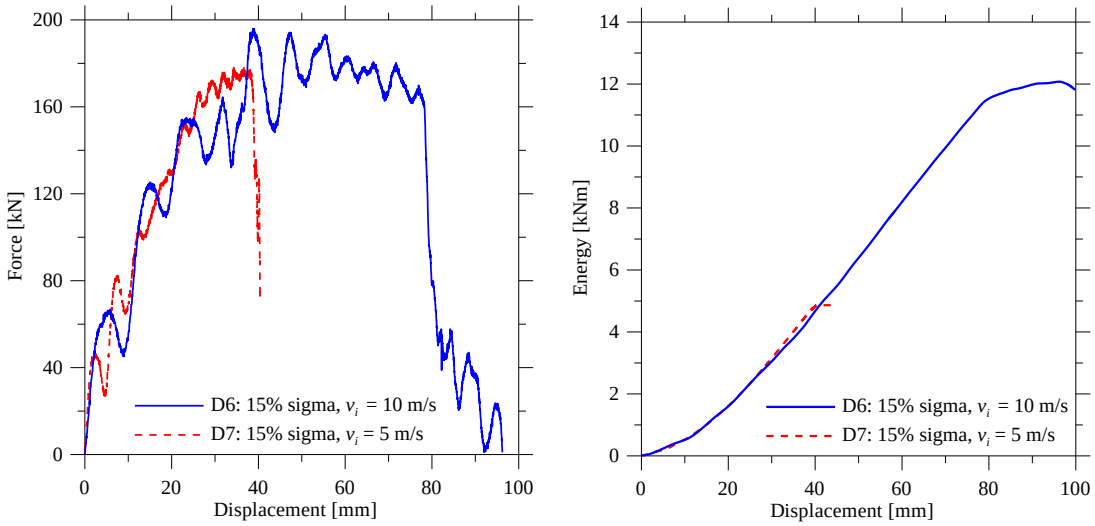

Fig. 13. Force-displacement and energy-displacement curves from test D6 and D7 at impact velocities of 10 m/s and 5 m/s.

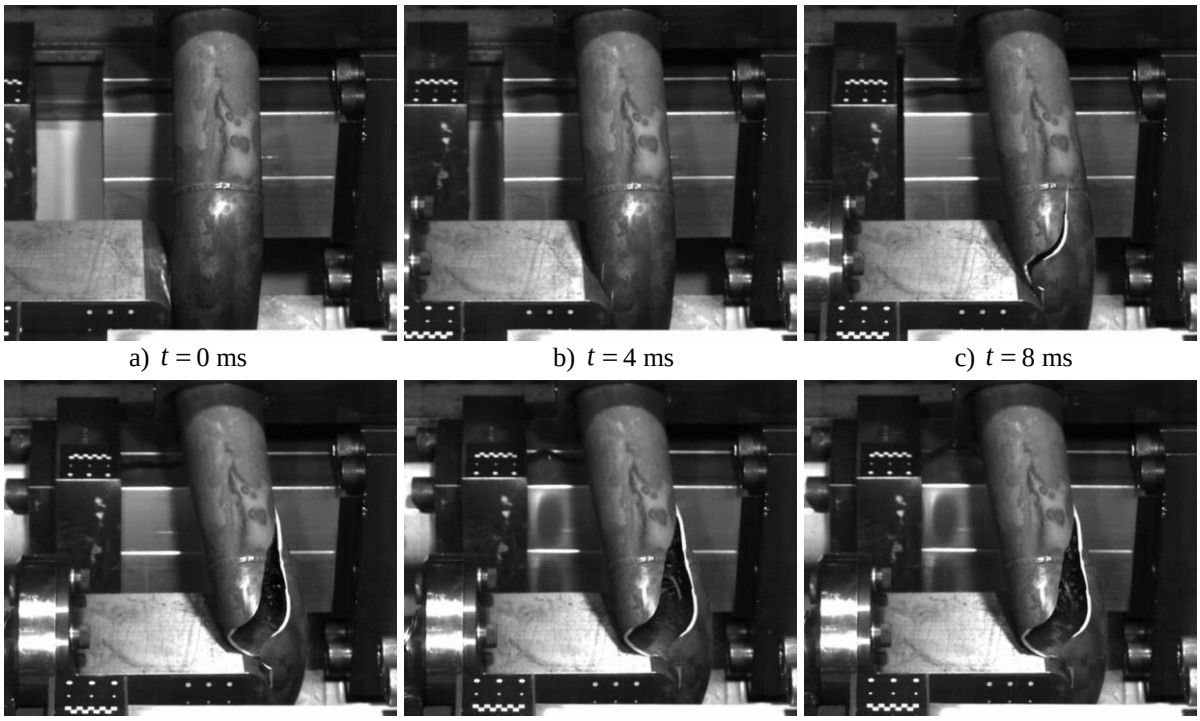

a) $t = 0$ ms b) $t = 4$ ms c) $t = 8$ ms

d) $t = 12$ ms e) $t = 16$ ms f) $t = 20$ ms

Fig. 14. High-speed camera images of impact process from dynamic test D6 ($\sigma \approx 15$ vol%, $v_i = 10$ m/s).

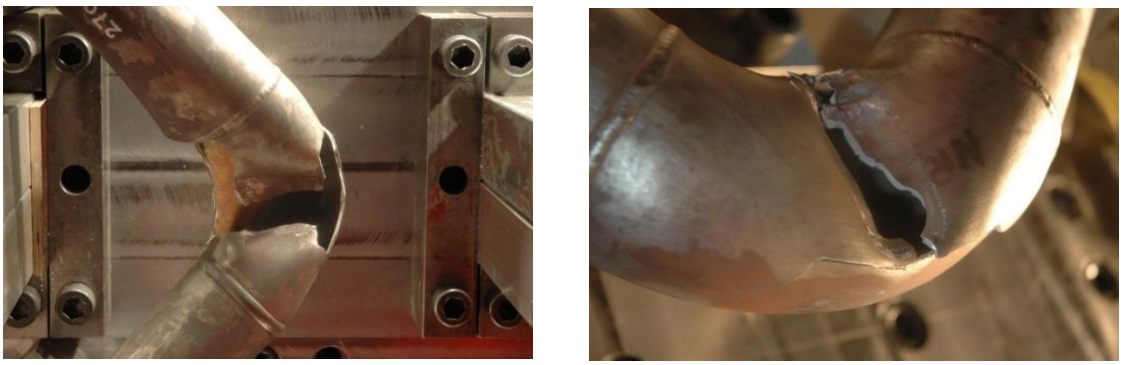

a) b)

Fig. 15. Final deformed shape of fittings after dynamic testing: a) Test D6 ($\sigma \approx 15$ vol%, $v_i = 10$ m/s); b) Test D7 ($\sigma \approx 15$ vol%, $v_i = 5$ m/s).

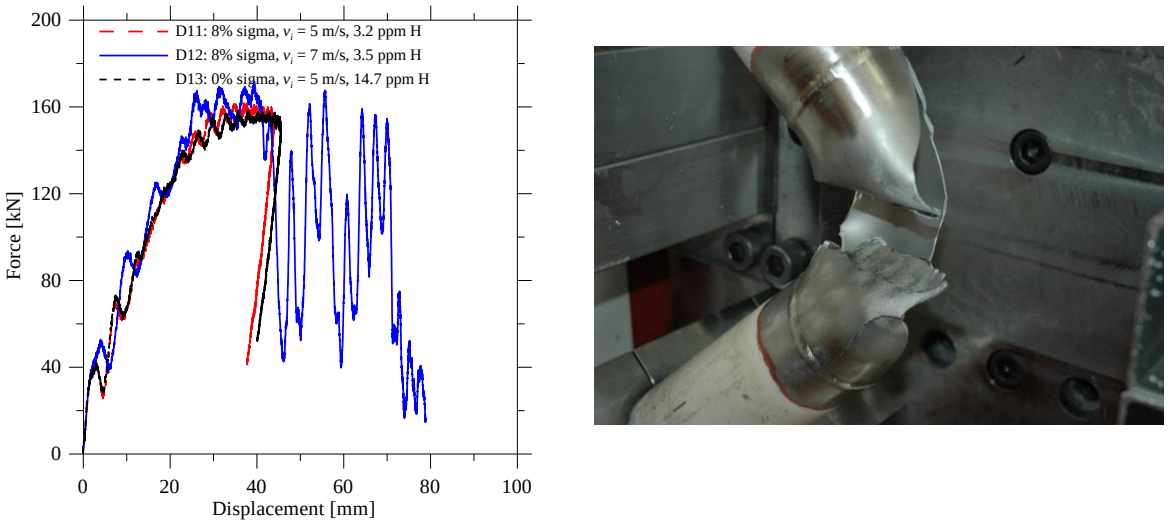

Fig. 16. Dynamic tests D11-D13 on hydrogen-charged fittings: a) Force-displacement curves; b) Fracture in test D12 ($\sigma \approx 8$ vol%, $v_i = 7$ m/s).

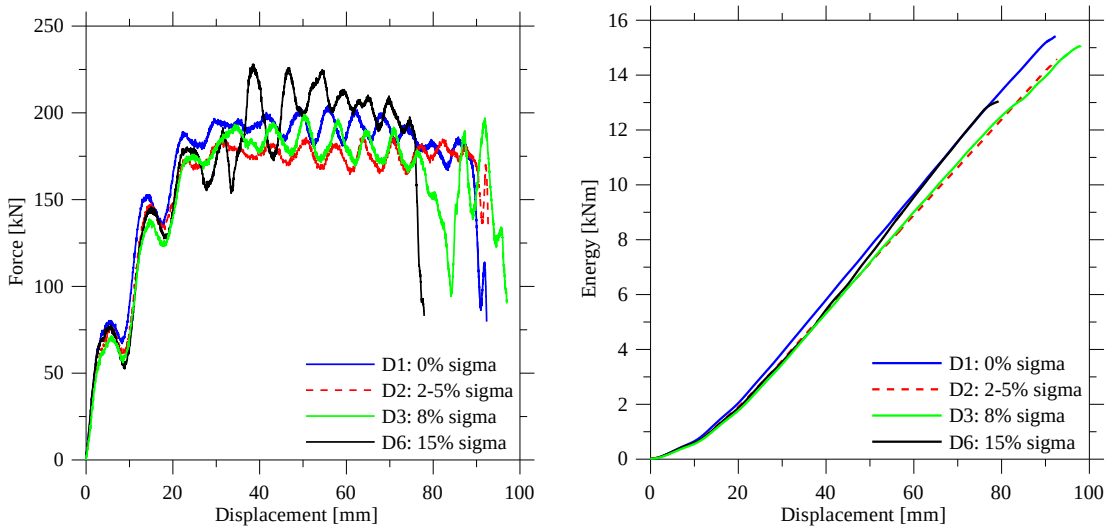

Fig. 17. Force-displacement and energy-displacement curves from impact tests on 3” pipes with various sigma phase levels at a constant impact velocity of 10 m/s.

Table 1. Mechanical data from quasi-static tensile tests at room temperature.

Amount of sigma [vol.%]	Initial thickness [mm]	Yield strength $\sigma_{0.2}$ [MPa]	Tensile strength σ_u [MPa]	Strain at max. load ε_u [mm/mm]	Uniaxial peak true stress σ_{pt} [MPa]	True strain at fracture ε_f [mm/mm]
~ 0	3.03	525	766.4	0.305	1586.0	1.519
~ 0	3.02	520	764.3	0.316	1547.6	1.388
~ 0	3.01	510	760.8	0.321	1535.2	1.388
1-5	3.03	550	791.4	0.251	1446.1	1.072
1-5	3.03	549	797.7	0.256	1518.4	1.180
~ 10	3.05	624	842.5	0.200	1355.6	0.685
~ 10	3.06	582	833.8	0.205	1349.2	0.728

Table 2. Experimental programme and results.

Test number	Loading rate	Pipe size	Assumed sigma phase level	Counted sigma phase level*	Hydrogen content	Fracture
QS1	2 mm/min	3"	~0 vol.%	N/A	0 ppm	No
QS2	2 mm/min	3"	2-5 vol.%	N/A	0 ppm	No
QS3	2 mm/min	3"	~8 vol.%	N/A	0 ppm	Crack
QS4	2 mm/min	3"	~15 vol.%	N/A	0 ppm	Yes
D1	10 m/s	3"	~0 vol.%	0.0 (0.0)	0 ppm	No
D2	10 m/s	3"	2-5 vol.%	4.3 (1.5)	0 ppm	No
D3	10 m/s	3"	~8 vol.%	9.6 (1.9)	0 ppm	Yes
D4	7 m/s	3"	~8 vol.%	N/A	0 ppm	Yes
D5	5 m/s	3"	~8 vol.%	9.9 (2.9)	0 ppm	Crack
D6	10 m/s	3"	~15 vol.%	14.4 (2.8)	0 ppm	Yes
D7	5 m/s	3"	~15 vol.%	14.9 (2.9)	0 ppm	Yes
D8	5 m/s	2"	1-2 vol.%	N/A	0 ppm	No
D9	10 m/s	2"	~0 vol.%	N/A	0 ppm	No
D10	10 m/s	2"	1-2 vol.%	N/A	0 ppm	No
D11	5 m/s	3"	~8 vol.%	8.5 (2.4)	3.2 ppm	Crack
D12	7 m/s	3"	~8 vol.%	10.1 (1.8)	3.5 ppm	Yes
D13	5 m/s	3"	~0 vol.%	0.0 (0.0)	14.7 ppm	No

* Standard deviation (SD) in brackets.